Chemical and physical transfers in an ultramafic rock weathering profile: Part 1. Supergene dissolution of Pt-bearing chromite

Daouda Traoré, Anicet Beauvais, François Chabaux, Chantal Peiffert, Jean-Claude Parisot, Jean-Paul Ambrosi, Fabrice Colin

Revision 1 (including editorial corrections)

Chemical and physical transfers in an ultramafic rock weathering profile: 1. Supergene dissolution of Pt-bearing chromite

Daouda Traoré [1,2], Anicet Beauvais [1,2,*], François Chabaux [3], Chantal Peiffert [4], Jean-Claude Parisot [1,2], Jean-Paul Ambrosi [2], Fabrice Colin [1,2]

[1] *Institut de Recherche pour le Développement (IRD), UMR 161 CEREGE, BP A5, 98848 Nouméa, Nouvelle-Calédonie*

[2] *Centre Européen de Recherche et d'Enseignement des Géosciences de l'Environnement, (UMR CNRS 6635 / UMR IRD 161), Aix-Marseille Université, Université Paul Cézanne, BP 80, 13545 Aix en Provence Cedex 4, France*

[3] *EOST-Centre de Géochimie de la Surface (CNRS/ULP), Université Louis Pasteur, 1 rue Blessig, 67084 Strasbourg Cedex, France*

[4] *UMR G2R/CREGU, Université Henri Poincaré 54506 Vandoeuvre-lès-Nancy, France*

*Corresponding author: Anicet.beauvais@noumea.ird.nc (Tel/Fax: (687) 26 07 59/67)

ABSTRACT

Chemical weathering and supergene dissolution processes of platinum-bearing chromite are studied in a lateritic weathering profile developed at the expense of ultramafic rocks in New Caledonia (Southwest Pacific). The chemical distributions of alkaline earth, transition metals and precious metals, including Pt and Pd are determined in a weathering profile varying from bedrock at the base upward through coarse and fine saprolites, and capped by a mottled zone and a lateritic colluvial nodular horizon. Chemical analyses and mass balance calculations suggest that progressive weathering of the parent rock is characterized by an enrichment of Fe, Co, and Mn, segregation of Ni at the transition between the bedrock and the coarse sapolite and in the lower part of the fine saprolite, and a depletion of Mg, Ca, Si, Al, and Cr. The higher concentrations of transition metals at the interface between the coarse and fine saprolite is due to vertical transfers and precipitation at the base of the weathering profile. In such a lateritic environment, the Pt-bearing chromite grains are progressively dissolved and the platinum group minerals (PGM) are released in the weathering mantle with a preferential depletion of palladium with regard to platinum.

Keywords: Lateritic weathering, ultramafic rocks, mass balance calculation, Pt-chromite, New Caledonia

INTRODUCTION

Lateritic weathering of rocks is one of the major processes that modify the earth's surface and contribute to the geochemical cycle of elements (Marker et al. 1991; Compton et al. 2003). It affects numerous regions of the intertropical zone (Pedro 1968; Nahon 1986; Tardy and Roquin 1992; Tardy 1997), where long-term chemical weathering has led to the dissolution of primary minerals including heavy minerals like metal-bearing spinel that results in supergene formation and accumulation of secondary and residual minerals in profiles of 10 to 100 m in thickness. The mobilization and recycling of chemical elements during supergene weathering processes is complex, depending on dissolution kinetics of primary minerals, formation of secondary phases, Eh-pH conditions, mass transfers and co-precipitation and ionic exchanges between various minerals (Harris and Adams, 1966; Nesbitt 1979; Cramer and Nesbitt 1983; Nahon 1991; Nesbitt and Wilson 1992; Islam et al. 2002). We study here the chemical weathering of ultramafic rocks of New Caledonia and particularly the supergene dissolution of platinum-bearing chromite grains disseminated in the weathering profile to characterize the weathering processes of the parent rocks and the release mechanism of platinum group minerals (PGM) in the weathering profile.

More than one-third of the area of New Caledonia is covered by ultramafic rocks, which are remnants of a Late Eocene overthrust belt now dissected by erosion (Paris 1981). These ultramafic rocks are deeply weathered, resulting in progressive leaching of Mg and Si and relative concentration of Fe and other metals in thick weathering profiles (Trescases 1975; Latham 1986). Ultramafic rocks are mainly harzburgite or lherzolite, which can exhibit serpentinization at their base; these rocks are also intercalated with dunite layers (Trescases 1975). Chromium spinel $(Mg, Fe^{2+})(Cr, Al, Fe^{3+})_2O_4$ is present interstitially up to 3% (Guillon 1975) or in pure chromite deposits of the ophiolitic harzburgites (Cassard et al. 1981; Augé 1985; Leblanc 1995). This primary chromite is

subsequently mobilized in eluvial and alluvial deposits. Significant proportions of this mineral have been previously reported in New Caledonian ophiolitic complexes, but the secondary supergene evolution of chromium spinel is poorly understood (Phan and Routhier 1964). A petrological and geochemical study of lateritic weathering profiles can contribute to improve this knowledge, and more particularly to address the specific metallogenic issue of the supergene weathering processes of platinum-bearing chromite.

GEOLOGICAL SETTING

The study area is located in the downslope part of the Pirogues River drainage basin in Southern New Caledonia (Fig. 1). The lithological units of this area consist of ultramafic rocks as cumulates of dunite, wehrlite and pyroxenite, and also harzburgites, which are serpentinized and cross-cut by pyroxenite dikes (Fig. 1). Platiniferous chromite are primarily concentrated either as stratiform accumulations in dunite and wehrlite or are disseminated in pyroxenite dikes and wehrlite. Most of the PGM are included in chromite (Augé and Maurizot 1995). Chromite forms thin schlieren and layers a few centimeters thick and a meter or so long in dunite and wehrlite cumulates. Irregular concentrations of massive chromite form ore in the pyroxenite dikes (Augé and Maurizot 1995). Chromite is crystallized in between large grains of pyroxene. Massive chromitite was also observed in the different horizons of the weathering profiles.

The ultramafic rocks are deeply weathered under the influence of a warm and humid climate characterized by a mean annual rainfall of 1700 mm with a wet season occurring from December to August. The ultramafic bedrock is generally overlain by a thick lateritic weathering mantle consisting typically from the base to the top (Trescases 1975; Besset 1980; Latham 1986; Llorca 1986) of: a coarse saprolite comprised of parent rock blocks, surrounded by weathering cortices; a fine saprolite where the silicates are totally hydrolyzed but the parent rock structure is preserved; a mottled zone composed of some

ferruginous nodules embedded in a goethitic matrix crossed by numerous millimeter-scale bioturbations; a soft nodular layer consisting mainly of millimeter to centimeter size nodules and pisoliths, and ferricrete fragments embedded in a red goethitic ferruginous matrix; a ferricrete exhibiting a massive, alveolar, and/or pisolitic structure, which is essentially composed of goethite and hematite. The parental structures are generally blurred in the ferruginous upper horizons.

Natural weathering profiles exposed in deep gullies (also locally called “lavakas”) have been described and sampled *in situ* (Fig. 2) for mineralogical and geochemical studies.

MATERIAL AND METHODS

Fourteen samples of parent rock, laterite and soil were collected *in situ* for measuring the bulk and grain density (Figs. 2 and 3). These samples were analyzed to determine (1) major element composition by Inductively Coupled Plasma - Atomic Emission Spectroscopy (ICP-AES) and (2) trace and precious metals by Inductively Coupled Plasma - Mass Spectrometry (ICP-MS). For ICP-AES analyses, the samples were crushed and finely ground (≤ 75 μm) after oven drying to be decomposed with 10 times their weight of a composite flux comprising 65% metaborate and 35% tetraborate according to the ME-ICP93 analytical procedure developed by the Australian Laboratory Services (ALS, Chemex). The resulting melts were dissolved in dilute nitric acid. Repeated fusion of finely ground powder was necessary to obtain complete decomposition of chromite, particularly for the samples containing coarser-grained chromite. For ICP-MS analysis of precious metals (Pt and Pd) each ground sample was fused with a mixture of lead oxide, sodium carbonate, borax and silica, inquarted with 6 mg of gold-free silver and then cupelled to yield a precious metal bead according to the PGM-MS23 analytical procedure developed by ALS Chemex, Australia. After cupellation the bead was dissolved in nitric and hydrochloric

118 acids and the solution diluted to volume. Detection limits for Pd and Pt are 1 and 0.5
119 ppb, respectively. X-ray diffraction (XRD) determinations were also processed on each
120 sample. Semi-quantitative proportions of minerals were deduced by the measurements of
121 the surface of main peaks in XRD spectra.

122 Three samples of 50 kg were also collected in the friable layers of the weathering profile
123 (fine saprolite, mottled zone and nodular layer). The samples were carefully washed, sifted to
124 1 mm and panned in order to separate out the heaviest particles. Chromite grains were
125 separated from the other heavy minerals under a binocular microscope for morphological
126 examination by scanning electron microscopy (SEM). After the SEM observation, chromite
127 grains were mounted with resin and polished sections were prepared for electron microprobe
128 analyses. Microanalyses of chromite grains were obtained using a Cameca SX 100 electron
129 microprobe with an acceleration potential of 15 keV, a beam current of 50 nA and counting
130 time of 10 s. The standards used were olivine for Mg, albite for Al, hematite for Fe,
131 orthoclase for Si, Cr_2O_3 for Cr, $MnTiO_2$ for Mn and Ti, NiO-466.6 for Ni, ZnO for Zn and
132 synthetic Co for Co.

133 ## RESULTS AND DISCUSSION

134 ### Physical and geochemical characterization

135 **Density and porosity change**. The weathering profile is developed from a wehrlite
136 type ultramafic rock (40-70% olivine, 30-45% antigorite and 10-20% diopside), and its
137 thickness is up to 4 meters. At the base of the profile (Fig. 2), the greenish-black parent
138 rock (-470 to -400 cm) changes to a brownish coarse saprolite (-400 to 290 cm) that
139 preserves parental structure and texture. Above (-290 to -100 cm) a yellow fine saprolite
140 is overlain by a red mottled zone (-100 to -60 cm) and a colluvial nodular horizon close
141 to the ground surface (Fig. 2), which is composed of ferruginous nodules, pisolites and
142 fragments of a previous ferricrete.

143 Rock porosity is an important physical parameter of weathering mantles as it controls soil,
144 water and air circulation, and thus permeability. Therefore, pores are a first order factor
145 controlling erosion and mass movement processes. In the profile studied, the bulk density
146 decreases from an average 2.37 $g.cm^{-3}$ in the fresh wehrlite to 1.32 $g.cm^{-3}$ in the coarse
147 saprolite, 0.93 $g.cm^{-3}$ and 1.13 $g.cm^{-3}$ in the fine saprolite and mottled zone, respectively, and
148 1.71 $g.cm^{-3}$ in the nodular horizon (Fig. 3a and Table 1). The grain density slightly increases
149 from an average 3.05 $g.cm^{-3}$ in the parent rock and the coarse saprolite, 3.58 $g.cm^{-3}$ in the fine
150 saprolite and 3.64 $g.cm^{-3}$ in the mottled zone to 3.67 $g.cm^{-3\ 3}$ in the nodular horizon (Fig. 3b
151 and Table 1). The porosity change is thus very important, from 22% in the fresh wehrlite to
152 56%, on average, in the coarse saprolite, 74% in the fine saprolite, 69% in the mottled zone,
153 and 53% in the upper nodular layer (Fig. 3c and Table 1).
154 **Petrologic and geochemical patterns.** The XRD mineralogical characterization of each
155 horizon composing the weathering profile indicates the presence of olivine, antigorite,
156 diopside and goethite with accessory chromite and enstatite. In the saprolites, the
157 silicates are progressively replaced by goethite, olivine being the first affected by
158 weathering. The coarse saprolite is composed of 30% olivine (up to 50% in the parent
159 rock), 40% antigorite (35% in the parent rock), 15% diopsite, 15% goethite. The base of
160 the fine saprolite is composed of 15% olivine, 5% antigorite, 10% diopside (15% in the
161 parent rock) and 50% goethite. At the top of the fine saprolite olivine, antigorite and
162 diopside are completely replaced by goethite, which reaches 100%. The mottled zone
163 and the nodular layer are essentially composed of goethite with accessory hematite and
164 chromite.
165 The geochemical analyses of the unweathered wehrlite indicate, on average, 39.6
166 wt.% SiO_2, and 34.70 wt.% MgO, and 19.3 wt.% Fe_2O_3 (Table 1). Silica decreases to
167 21.2 wt.% at the top of the coarse saprolite and MgO to 7.1 wt.%. Iron (III) oxide

contents increase, on average, from 19.3 wt.% to 45.2 wt.%. Aluminum and chromium contents do not significantly change between parent wehrlite and coarse saprolite: on average, 0.6 – 0.7 wt.% Al_2O_3, 1.5 – 2.3 wt.% Cr_2O_3. The transition metal contents increase, on average, from 1.97 $g.kg^{-1}$ to 4.40 $g.kg^{-1}$ for Mn, 0.23 $g.kg^{-1}$ to 0.48 $g.kg^{-1}$ for Co, and 0.34 $g.kg^{-1}$ to 0.53 $g.kg^{-1}$ for Ni (Table 1).

The coarse saprolite is progressively transformed into a fine saprolite, in which the texture and the structure of the parent rock are still preserved. On average, the geochemical analyses of the fine saprolite indicate 3.4 wt.% SiO_2, 0.9 wt.% Al_2O_3, 77 wt.% Fe_2O_3, 3.3 wt.% Cr_2O_3, 0.04 wt.% CaO, 0.85 wt.% MgO, 8.3 $g.kg^{-1}$ Mn, 2.8 $g.kg^{-1}$ Co, and 8.2 $g.kg^{-1}$ Ni (Table 1).

Toward the top of the profile, the fine saprolite changes to a bioturbated-mottled laterite in which the original rock structure is no longer preserved. The chemical composition is similar to the one analyzed in the upper part of the fine saprolite except for decreased Co content (Table 1).

Mass balance calculations

Mass balance calculations related to weathering processes require the application of rigorous means to estimate losses or gains based on a thorough petrological study (Millot and Bonifas 1955; Gresens 1967; Brimhall and Dietrich, 1986; Colin et al. 1992, 1993; Beauvais and Colin 1993). The parental rock structures are well preserved in the saprolite suggesting that weathering processes have preserved the original volume. Based on the assumption that the volume has not varied between bedrock (-470 cm) and the top of the fine saprolite (-110 cm), isovolume mass-balance calculations can be applied to quantify mass transfers induced by the transformation of parent-rock into saprolite (Millot and Bonifas 1955). Numerous authors have mathematically formalized mass balance calculations (Gresens 1967; Brimhall and Dietrich 1986) by a functional

form of the constitutive relationships between the chemical compositions of parent and weathered material, their bulk densities, and volumes. The net gains and losses of chemical constituents are calculated from the following equation (Brimhall and Dietrich 1986):

$$K_j = \left[\left(\frac{C_{jw} \times \rho_{jw}}{C_{jp} \times \rho_{jp}}\right) - 1\right] \times 100, \quad (1)$$

where K_j is the gain and/or loss factor of chemical element j ; C_{jw} and C_{jp} are the chemical element j concentrations (expressed in $g.kg^{-1}$ for Si, Al, Fe, Ca, Mg and Cr, or $mg.kg^{-1}$ for Mn, Co and Ni) in the weathered layer, w, and the parent material, p, respectively; and ρ_{jw} and ρ_{jp} are bulk densities of the weathered material, w, and the parent material, p, respectively (expressed in $g.cm^{-3}$).

The total mass (m_{jw}) of each element j gained or lost during the weathering process is calculated from the following equation (Colin et al. 1993):

$$m_{jw} = C_{jp} \times \rho_{jp} \times V_p \times K_{jw}, \quad (2)$$

where V_p is the volume of the parent rock (V_p = 1 m^3), K_{jw} is the gain and/or loss factor of chemical element j in the weathered layer, w, calculated from the equation (1), and C_{jp}, ρ_{jp} and m_{jw} are expressed in $kg.ton^{-1}$, $ton.m^{-3}$ and $kg.m^{-3}$, respectively.

Mass balance calculations show that 96% Si, 99% Mg, 94% Ca have been depleted in the fine saprolite (Table 2a and Fig. 4) that corresponds, on average, to mass transfers of -426 kg Si, -488 kg Mg and -5.4 kg Ca per cubic meter of weathered parent rock (Table 2b). This is accompanied, on average, by 47% loss of Al and 16% loss of Cr, i.e., -4 $kg.m^{-3}$ Al and -4

217 kg.m^{-3} Cr, the highest values being recorded at the base of the fine saprolite (Table 2 and
218 Figs. 4a and 4c). Iron, Mn, and Co contents are enriched at the top of the coarse saprolite only
219 by 4.7% (+17.2 kg.m^{-3}), 8% (+0.39 kg.m^{-3}), and 9% (+0.05 kg.m^{-3}), respectively, while Ni is
220 slightly depleted by -10% (-0.69 kg.m^{-3}) (Fig. 4 and Table 2). At the base of the fine
221 saprolite, the enrichment rates strongly increase by 30% (+110 kg.m^{-3}) for Fe, 45% (+3.18
222 kg.m^{-3}) for Ni, 54% (+2.61 kg.m^{-3}) for Mn, and 458% (+2.35 kg.m^{-3}) for Co. At the top of
223 the fine saprolite, the enrichment rates are 38% (+142 kg.m^{-3}) for Fe, 81% (+3.9 kg.m^{-3})
224 for Mn and 312% (+1.6 kg.m^{-3}) for Co, while Ni is depleted by -20% (-1.38 kg.m^{-3})
225 (Table 2a and 2b).

226 The sharp decrease of Si, Mg and Ca contents (from parent rock to saprolite) reflects the
227 congruent weathering of primary silicates (Eggleton et al. 1987; Nesbitt and Wilson 1992;
228 Islam et al 2002). The weathering creates high porosity and resultant improved drainage
229 conditions if pore spaces are interconnected (Trescases 1975; Latham 1986; Marker et al.
230 1991). The Fe-enrichment at the transition between coarse and fine saprolite (Fig. 4a and
231 Table 2) is due to relatively short vertical migrations of iron in the weathering profile that has
232 led to goethite formation, which may have trapped transition metals such as Mn, Co and Ni
233 (Millot and Bonifas 1955; Tardy and Roquin 1992; Beauvais and Colin 1993; Beauvais and
234 Roquin 1996).

235 The primary host minerals for Ni in the ultramafic rocks are olivine, serpentine and
236 accessory pyroxene (Zeissink 1969; Trescases 1975; Besset 1980; Colin et al. 1990; Gaudin,
237 2002). During the weathering of these parent minerals in strong oxidizing conditions, Ni is
238 mobilized and enriched by co-precipitation with secondary Fe and Mn oxides at the transition
239 between the coarse and fine saprolite (Fig. 4c and Table 2) as previously shown (Schellmann
240 1981; Golightly 1981; Elias et al. 1981; Trescases 1975; Reimann and Caritat 1998).

241 Manganese enrichment in the fine saprolite (on average, +60%), as compared to its content
242 in the parent rock (Table 2a), can be explained by significant vertical and/or lateral transfers
243 of Mn, which is released as Mn^{2+} in the saturated zone of the deeper saprolite (Golightly
244 1979). Vertical transfers may be due to the leaching of Mn from the near-surface part of the
245 profile under conditions of low pH and high CO_2 activity. These environmental conditions
246 favor reduction of Mn^{4+} to Mn^{2+} (Golightly 1979; Beauvais et al. 1987). Colloidal Mn^{2+}
247 complexes are highly mobile and can be transported in the soils over long distances
248 (Krauskopf 1979; Marker et al. 1991). As soon as Mn-bearing solutions reach the lower part
249 of the weathering profile, rising pH due to silicate hydrolysis and increased concentration of
250 the solution above the saprolite, are likely to result in the oxidation of Mn^{2+} and precipitation
251 of Mn oxides from the colloidal solution (Trescases 1975; Golightly 1979; Llorca 1986;
252 Marker et al. 1991).
253 The behavior of Co is also controlled by physical-chemical properties of the downward-
254 migrating solutions (Marker et al. 1991). Cobalt is adsorbed by negatively charged Mn^{4+}
255 colloids and/or incorporated into Mn oxides (Burns 1976; Manceau et al. 1987; Llorca and
256 Monchoux 1991; Llorca 1993). Precipitation of Co at the base of the profile, where pH is
257 higher, is more effective, because the solubility product of Co hydroxide is lower than that of
258 Mn hydroxide (Trescases 1975; Schellmann 1978; Golightly 1981). This property can explain
259 the higher enrichment factor of Co (+450%) compared to Mn (+54%) or Ni (+45%) in the
260 lower cementation zone (Figs. 4c and d, Table 2) (Marker et al. 1991).
261 The Cr-bearing minerals in the ultramafic rocks are mainly chromite and accessory silicate
262 minerals. Chromium-bearing silicate minerals are, however, depleted in the upper saprolite.
263 Some Cr may be leached downward in the form of $Cr(OH)_3$ in alkaline environments (Marker
264 et al. 1991). Chromium within chromite is generally considered immobile in supergene
265 environments (Trescases 1975; Schellmann 1978; Becquer et al. 2003). However, recent

thermodynamic and field studies have shown that chromite is soluble in lateritic environments (Fendorf 1995), suggesting that Cr in laterites derived from the weathering of ultramafic rocks may be depleted from the profile. As chromite is the main host mineral of aluminum in the wehrlite, its solubility also explains the depletion of Al in the profile.

Supergene dissolution of chromite

The chemical compositions of chromite from different samples of Pt-rich chromitite of the Pirogues site are plotted in Figure 5, together with disseminated chromite from the cumulate series, and chromitite from previously studied mantle deposits (Augé and Maurizot 1995), as, for example, those from the Tiebaghi massif in northwestern New Caledonia, in which the chromite has a very constant composition (high Cr^{3+} (55.5-63.5 wt.% Cr_2O_3) and low Fe^{3+} (1.5-4.3 wt.% Fe_2O_3)). Chromite disseminated in mineralized cumulates is slightly impoverished in Cr (Fig. 5). Platinum-bearing chromite concentrations in the cumulate series of the Pirogues area differ significantly from those of mantle chromitite in having relatively low Cr^{3+} (40-46 wt.% Cr_2O_3) and high Fe^{3+} (10-17 wt.% Fe_2O_3) (Fig. 5). No significant difference was observed between chromitite of pyroxenite dikes and chromitite of cumulates.

The platinum-bearing chromite in the parent rock and coarse saprolite is euhedral (Fig. 6a), with surfaces that may represent small primary dissolution cracks (Fig. 6b). The progressive weathering of chromite is illustrated in Figure 6. In the fine saprolite, where the lowest bulk densities and the highest porosities were measured (Fig. 3 and Table 1), the dissolution of chromite starts along the primary cracks and increases until forming a network of etching pits of sub-micrometric size (Fig. 6c and 6d). This effectively corresponds to the highest losses of Cr (Fig. 4c and Table 2). In the mottled zone, residual chromite grains with smooth edges are embedded in ferruginous aggregates and/or pisolites (Fig. 6e), which are essentially composed of goethite. The dissolution front increases in the chromite by widening of microcracks and fissures hosting weathering solutions (Fig. 6f). The supergene dissolution

process leads to the dislocation of chromite crystals in the superficial layers (Fig. 6g and 6h). Chromite grain dissolution in supergene environments is driven by an hydrolysis process that produces $Cr(OH)_3$ (Cooper 2002) via:

$$FeCr_2O_4 + 2H_2CO_3 + 2H_2O = Fe^{2+}_{aq} + 2Cr(OH)_3 + 2HCO_3^- \quad (3)$$

The production of $Cr(OH)_3$ requires moist, slightly reduced conditions to keep Fe(II) ions in solution, such as those prevailing in the fine saprolite, which is characterized by an unconnected fine porosity and poor drainage. The $Cr(OH)_3$ produced can be adsorbed to the surface of the crystal structure of iron and/or manganese oxyhydroxides (McKenzie 1977; Manceau and Charlet 1992; Fendorf 1995).

The dissolution reaction of $Cr(OH)_3$ to produce soluble Cr(III) ions is represented by :

$$Cr(OH)_3 + 3H^+ = Cr^{3+}_{aq} + 3H_2O \quad (4)$$

This reaction is possible only under strongly acidic conditions with pH values lower than 4 (Fendorf 1995; Cooper 2002). Such conditions prevail at the top of lateritic profiles, which is often rich in organic matter.

The poorly-aerated chromite-rich ferruginous aggregates can also undergo oxidation-reduction conditions that favor the hydrolysis of Cr(III) into $Cr(OH)_3$ (Cooper 2002). The dissolution of chromite ultimately leads to the release of PGM initially included in chromite crystals.

Residual origin of platinum

Decoupling of platinum group elements, Pt and Pd, and variation of the ratio Pt/Pd, are characteristic of the behavior of the PGE in supergene environments (Prichard and Lord 1994;

316 Evans et al. 1994; Oberthür et al. 2003). Between the bedrock and the upper part of the fine
317 saprolite, the Pt/Pd ratio is as high as the chromium is depleted (Fig. 7 and Tables 1 and 2).
318 The increase of Pt/Pd in the weathering profile reflects the preferential release of palladium
319 with regard to platinum (Varajao et al. 2000). Figure 7 also suggests that PGM could be
320 released concomitant with chromite dissolution and also, that the supergene dissolution of Pt-
321 bearing chromite and/or newly released PGM lead to a preferential depletion of Pd with
322 regard to Pt. The specific behavior of PGM in the lateritic weathering profile is addressed
323 separately (Traore et al. 2007).

324 **CONCLUSION**

325 Supergene dissolution of platinum-bearing chromite has been characterized in a lateritic
326 weathering profile from New Caledonia. Based on mass balance calculations, the results
327 document the spatial redistribution of chemical elements during chemical weathering
328 processes. Silicon, Mg and Ca are depleted entirely from the weathering profile resulting from
329 the chemical weathering of olivine, pyroxene and serpentine. The residual Fe forms iron
330 hydroxides, often crystallized into goethite, which can eventually trap other transition metals.
331 Manganese, Co and Ni form poorly crystallized secondary minerals such as Mn-asbolanes
332 and/or co-precipitate with iron hydroxides. The Cr-bearing silicates are dissolved and Cr is
333 leached out of the profile. Chromite dissolution induces Cr depletion and Al removal. This
334 investigation illustrates the decoupling of PGE and Cr content during the lateritic weathering
335 of Pt-bearing chromite and suggests that the platinum mineralization is globally residual. The
336 chromite dissolution may effectively contribute to the release of PGM in the profile with a
337 preferential depletion of palladium with regard to platinum.

338 **ACKNOWLEDGEMENTS**

339 This work is a contribution IRD-UMR161-CEREGE. Dr. P. Maurizot is thanked for
340 introducing us to the study area. Michel Cathelineau, Gaëlle Bouichet, Marc Brouand and

341 Philippe Larqué are gratefully acknowledged for their help during mineralogical
342 investigations. J. Butscher, D. Chardon, V. Chevillotte, V. Combier, A. Paugam, J. Perrier, N.
343 Perrier and B. Robineau are also thanked for their help during fieldwork. Dr. Giorgio Garuti,
344 Dr. Anthony Velbel and an anonymous reviewer are thanked for their helpful review of the
345 manuscript.
346

REFERENCES CITED

Augé, T. (1985) Chromite et minéraux du groupe du platine dans les complexes ophiolitiques. Caractérisation des séries hôtes. Thesis, 270 p., Université Orléans, orléans, France.

Augé, T., and Maurizot, P. (1995) Stratiform and alluvial platinum mineralization in the New Caledonia ophiolite complex. Canadian Mineralogist, 33, 1023-1045.

Beauvais, A. and Colin, F. (1993) Formation and transformation processes of iron duricrust systems in tropical humid environment. Chemical Geology, 106, 77-101.

Beauvais,, A., Melfi, A.J., Nahon, D., and Trescases, J-J. (1987) Pétrologie du gisement latéritique manganesifère d'Azul (Brésil). Mineralium Deposita, 22, 124-134.

Beauvais, A. and Roquin, C. (1996) Petrological differentiation patterns and geomorphic distribution of ferricretes in Central Africa. Geoderma, 73, 63-82.

Becquer, T., Quantin, C., Sicot, M., and Boudot, J.P. (2003) Chromium availability in ultramafic soils from New Caledonia. Science of Total Environment, 301, 251-261.

Besset, F. (1980) Localisation et répartitions successives du nickel au cours de l'altération latéritique des péridotites de Nouvelle-Calédonie. Mémoire du Centre d'Etudes et de Recherches Géologiques et Hydrologiques, 129 p., Tome XV, CERGA Ed., Montpellier, France.

Brimhall, G.H., and Dietrich, W.E. (1986) Constitutive mass-balance relations between chemical composition, volume, density, porosity and strain in metasomatic hydrochemical systems: results on weathering and pedogenesis. Geochimica et Cosmochimica Acta, 51, 567-587.

Burns, R.G. (1976) The uptake of cobalt into ferromanganese nodules, soils and synthetic manganese (IV) oxides. Geochimica et Cosmochimica Acta, 40, 95-102.

369 Cassard, D., Nicolas, A., Rabinovitch, M., Moutte, J., Leblanc, M., and Prinzhofer, A. (1981)
370 Structural classification of chromite pods in southern New Caledonia. Economic Geology,
371 76, 805-831.
372 Colin, F., Brimhall, G.H., Nahon, D., Lewis, C.J., Baronnet, A., and Danti, K. (1992)
373 Equatorial rain forest lateritic mantles: A geomembrane filter. Geology, 20, 523-526.
374 Colin, F., Nahon, D., Trescases, J.J, and Melfi, A.J. (1990) Lateritic weathering of
375 pyroxenites at Niquelandia, Goias, Brazil: The supergène behavior of nickel. Economic
376 Geology 85, 1010-1023.
377 Colin, F., Veillard, P., and Ambrosi, J.P. (1993) Quantitative approach to physical and
378 chemical gold mobility in equatorial rainforest lateritic environment. Earth and Planetary
379 Science Letters, 114, 269-285.
380 Compton, J.S., White, R.A., and Smith, M. (2003) Rare earth element behavior in soils and
381 salt pan sediments of a semi-arid granitic terrain in the Western Cape, South Africa.
382 Chemical Geology, 201, 239-255.
383 Cooper, G.R.C. (2002) Oxidation and toxicity of chromium in ultramafic soils in Zimbabwe.
384 Applied Geochemistry, 17, 981-986.
385 Cramer, J.J, and Nesbitt, H.W. (1983) Mass-balance relations and trace element mobility
386 during continental weathering of various igneous rocks. In S.G. Memory, Ed., p. 63-73.,
387 Symposium on Petrology of Weathering and Soils.
388 Eggleton, RA., Foudoulis, C., and Varkevisser, D. (1987) Weathering of basalt: changes in
389 rock chemistry and mineralogy. Clays and Clay Minerals, 35, 161-169.
390 Elias, M., Donaldson, M.J., and Giorgetta, N. (1981) Geology, mineralogy, and chemistry of
391 lateritic nickel-cobalt deposits near Kalgoorlie, Western Australia. Economic Geology, 76,
392 1775-1783.

393 Evans, D.M., Buchanan, D.L., and Hall, G.E.M. (1994) Dispersion of platinum, palladium
394 and gold from the main sulphide zone, Great Dike, Zimbabwe. Transactions of the
395 Institution of Mining and Metallurgy,103, (Section B: Applied earth science), B57-B67.
396 Fendorf, S.E. (1995) Surface reactions of chromium in soils and waters. Geoderma 67, 55-71.
397 Gaudin, A. (2002) Cristallochimie des smectites du gisement latéritique nickélifère de Murrin
398 Murrin (Ouest Australie). Ph D, 236 p. Université Aix-Marseille III, Marseille, France.
399 Golightly, J.P. (1979) Geology of Soroako nickeliferous laterite deposits. AIME International
400 Laterite Symposium, p. 38-55., New Orleans, USA.
401 Golightly, J.P. (1981) Nickeliferous laterite deposits. Economic Geology, 75th Anniversary
402 vol., 710-735.
403 Gresens, R.L. (1967) Composition-volume relations of metasomatism. Chemical Geology, 2,
404 47-65.
405 Guillon, J.H. (1975) Les Massifs péridotitiques de Nouvelle-Calédonie: type d'appareil
406 ultrabasique stratiforme de chaine récente. Mémoire ORSTOM 76 Paris, 113 p.
407 Harris, R.C., and Adams, J.A.S. (1966) Geochemical and mineralogical studies on the
408 weathering of granitic rocks. American Journal of Science, 264, 146-173.
409 Islam, M.R., Peuraniemi, V., Aario, R., and Rojstaczer, S. (2002) Geochemistry and
410 mineralogy of saprolite in Finish Lapland. Applied Geochemistry, 17, 885-902.
411 Krauskopf, K.B. (1979) Introduction to Geochemistry, 617 p. McGraw-Hill Tokyo.
412 Latham, M. (1986) Altération et pédogenèse sur roches ultrabasiques en Nouvelle-
413 Calédonie: genèse et évolution des accumulations de fer et de silice en relation avec la
414 formation du modelé. Etudes et Thèses, 331 p., ORSTOM, Paris, France.
415 Leblanc, M. (1995) Chromitite and ultramafic rock compositional zoning through a
416 paleotransform fault, Poum, New Caledonia. Economic Geology, 90, 2028-2039.

417 Llorca, S. (1986) Les concentrations cobaltifères supergènes en Nouvelle-Calédonie:
418 géologie, minéralogie. Thesis 90 p., Université Paul Sabatier, Toulouse, France.
419 Llorca, S. (1993) Metallogeny of supergene cobalt mineralization, New Caledonia. Australian
420 Journal of Earth Science, 40, 377-385.
421 Llorca, S., and Monchoux, P. (1991) Supergene cobalt minerals from New Caledonia.
422 Canadian Mineralogist, 29, 149-161.
423 Manceau, A., and Charlet, L. (1992) X-ray absorption spectroscopic study of the sorption of
424 Cr(III) at the oxide-water interface: I. Molecular mechanism of Cr(III) oxidation on Mn
425 oxides. Journal of Colloidal Interface Science, 148, 425-442.
426 Manceau, A., Llorca, S., and Calas, G. (1987) Crystal chemistry of cobalt and nickel in
427 lithiophorite and asbolane from New Caledonia. Geochimica et Cosmochimica Acta, 51,
428 105-113.
429 Marker, A., Friedrich, G., Carvalho, A., and Melfi, A. (1991) Control of the distribution of
430 Mn, Co, Zn, Zr, Ti, and REEs during the evolution of lateritic covers above ultramafic
431 complexes. Journal of Geochemical Exploration, 40, 361-383.
432 McKenzie, R.M. (1977) Manganese oxides and hydroxides. In J.B. Dixon, and S.B. Weed,
433 Eds., Minerals in Soil Environments, Soil Science Society of America, 181-193.
434 Millot, G., and Bonifas, M. (1955) Transformations isovolumiques dans les phénomènes de
435 latéritisation et de bauxitisation. Bulletin du Service de la Carte Géologique d'Alsace-
436 Lorraine, Strasbourg, 8, 8-10.
437 Nahon, D. (1991) Introduction to the Petrology of Soils and Chemical Weathering, 313 p.
438 Wiley Interscience, New York.
439 Nahon. D.B. (1986) Evolution of iron crusts in tropical landscapes. In S.H. Coleman, and
440 D.P. Dethier, Eds., Rates of Chemical Weathering of Rocks and Minerals, p. 169-187.
441 Academic Press Incorporation, San Diego.

442 Nesbitt, H.W. (1979) Mobility and fractionation of rare earth elements during weathering of
443 granodiorite. Nature, 279, 206-210.
444 Nesbitt, H.W., and Wilson, R.E. (1992) Recent chemical weathering of basalts. American
445 Journal of Science, 292, 740-777.
446 Oberthür, T., Weiser, T.W., and Gast, L. (2003) Geochemistry and mineralogy of platinum-
447 group elements at Hartley Platinum Mine, Zimbabwe. Mineralium Deposita, 38, 344-355.
448 Paris, J.P. (1981) Géologie de la Nouvelle-Calédonie: un essai de synthèse. Mémoire BRGM
449 113, Orléans, 278 p.
450 Pedro, G. (1968) Distribution des principaux type d'altération chimique à la surface du globe.
451 Présentation d'une esquisse géographique. Revue de Géographie Physique et Géologie
452 Dynamique, 10, 457-470.
453 Phan, K.D., and Routhier, P. (1964) Altération météorique de chromite de Nouvelle-
454 Calédonie: Etude à la microsonde électronique. Contribution à la géochimie supergène du
455 chrome en milieu latéritique. Conséquences pratiques pour la concentration des chromite
456 détritiques. Bulletin BRGM, 4, 111-133.
457 Prichard, M.H., and Lord, R.A. (1994) Evidence for differential mobility of platinum-group
458 elements in the secondary environnement in Shetland ophiolite complex. Transactions of
459 the Institution of Mining and Metallurgy, 103, (Section B; Applied earth science), B79-
460 B86.
461 Reimann, C., and de Caritat, P.D. (1998) Chemical elements in the environment. Factsheets
462 for the geochemist and environmental scientist, Springer Verlag Publication, Berlin.
463 Schellmann, W. (1978) Behavior of nickel, cobalt, and chromium in ferruginous lateritic
464 nickel ores. Bulletin BRGM, 2, 275-282.
465 Schellmann, W. (1981) Formation of nickel silicate ores by weathering of ultramafic rocks.
466 Development in Sedimentology, 35, 623-634.

467 Tardy, Y. (1997) Petrology of laterites and tropical soils, 459 p. Balkema, Amsterdam.
468 Tardy, Y., and Roquin, C. (1992) Geochemistry and evolution of lateritic landscapes. In I.P.
469 Martini, and W. Chesworth, Eds., Weathering, Soils & Paleosols, p 407-443. Elsevier
470 Publication, Amsterdam.
471 Traoré, D., Augé, T., Beauvais, A., Parisot, J.C., Colin, F., and Cathelineau, M. (2007)
472 Chemical and physical transfers in an ultramafic rock weathering profile: 2. Dissolution vs.
473 accumultion of platinum group minerals. American Mineralogist, submitted.
474 Trescases, J.J. (1975) L'évolution géochimique supergène des roches ultrabasiques en zone
475 tropicale: formation des gisements nickélifères de Nouvelle- Calédonie. Mémoire
476 ORSTOM 78, Paris, 280 p.
477 Varajao, C.A.C., Colin, F., Vieillard, P., Melfi, A.J., and Nahon, D. (2000) Early Weathering
478 of palladium gold under lateritic conditions, Maquine Mine, Minas Gerais: Brazil. Applied
479 Geochemistry, 15, 245-263.
480 Zeissink, H.E. (1969) The mineralogy and geochemistry of a nickeliferous laterite profile
481 (Greenvale, Queensland, Australia). Mineralium Deposita, 4, 132-152.
482

Figure and Table Captions

Figure 1. (a) Geological map and location of studied area (after Augé and Maurizot, 1995). The black star shows the location of the studied weathering profile (Fig. 2). (b) Inset of the main Island of New Caledonia with its ultramafic massifs and location of (a) by the black rectangle.

Figure 2. Weathering profile log from a crosscut into a natural gully ("lavaka") and the location of analyzed samples (white squares), the numbers of which being in italics.

Figure 3. (a) Bulk density, (b) Grain density and (c) Porosity variation along the profile.

Figure 4. Results of the geochemical mass balance calculation along the profile.

Figure 5. Chemical compositions of chromite from PGE-rich chromitite of the Pirogues River mineralization (black circles) and disseminated chromite in cumulate hosting the mineralization (grey circles). Light gray circles correspond to mantle chromitite from Tiébaghi (after Augé, 1985).

Figure 6. S.E.M. photomicrographs of the progressive weathering of chromite (a) euhedral grain of primary chromite in the coarse saprolite, (b) detail of a primary chromite grain surface showing dissolution cracks, (c) euhedral grain of chromite affected by a microdrain network in the red laterite, (d) etching dissolution pits of a chromite grain, (e) residual chromite grain in a ferruginous cortex, (f) detail of dissolution features of a chromite, (g) small size chromite grain disseminated in a pisolite, (h) detail of (g).

Figure 7. Comparison between the total mass transfer of Cr and Pt/Pd variation in the weathering profile.

510 TABLE 1. Physical and chemical characteristics of the parent rock, and the different

511 layers of the weathering profile (ρ_w = bulk density; ρ_g = grain density).

512

513 TABLE 2. Results of (a) the mass balance factor (K) and (b) the total mass transfer (m) of

514 chemical elements calculated from equation (1) and (2), respectively.

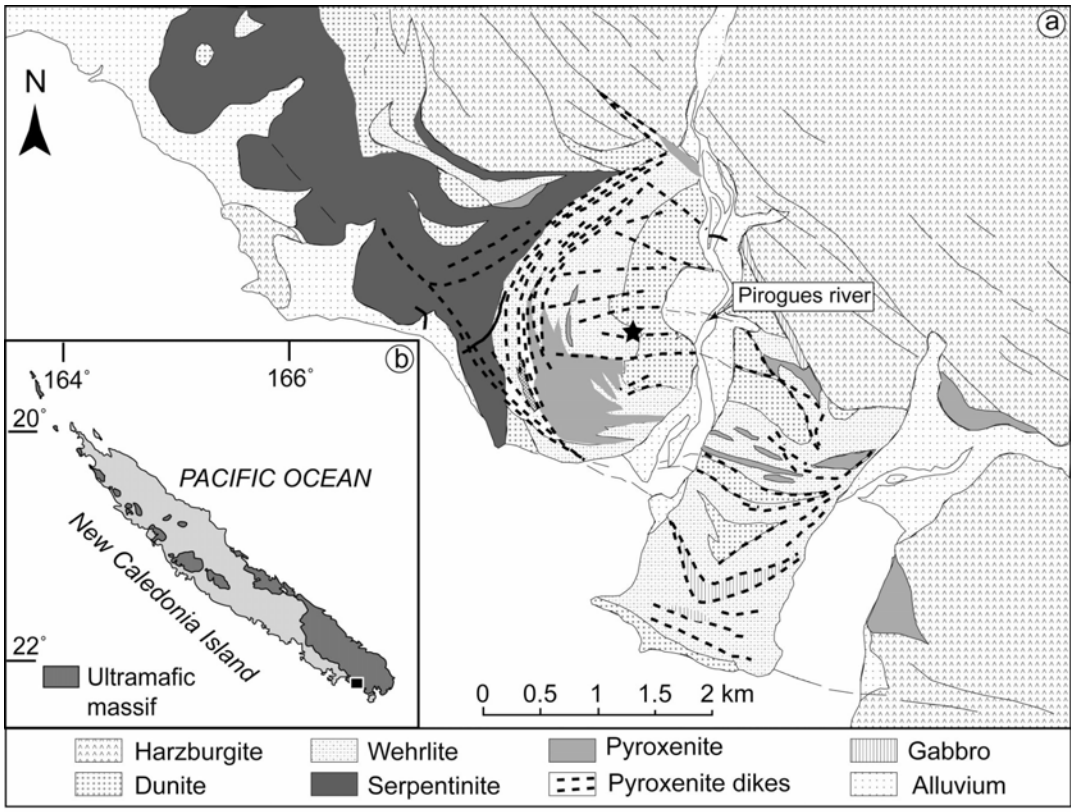

FIG. 1

Traore et al., 2007

520

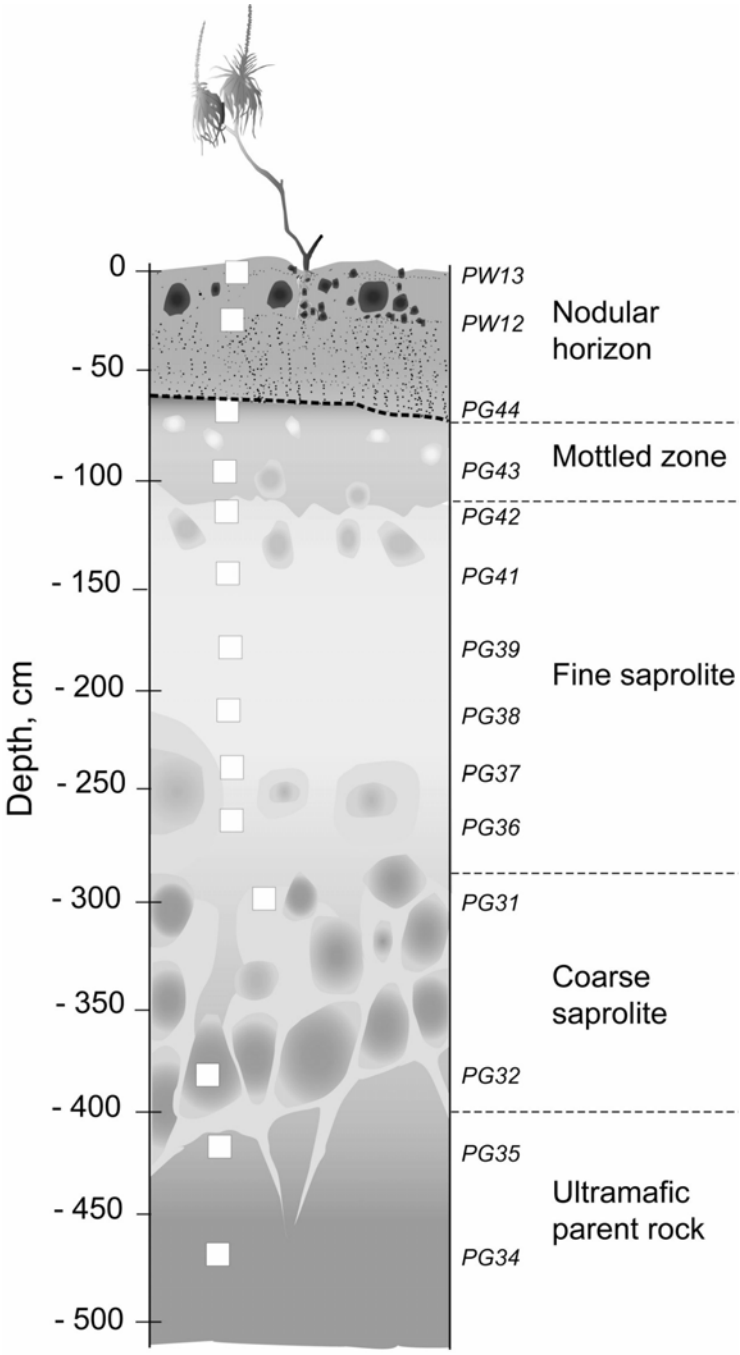

FIG. 2

Traore et al., 2007

521

522

522

523

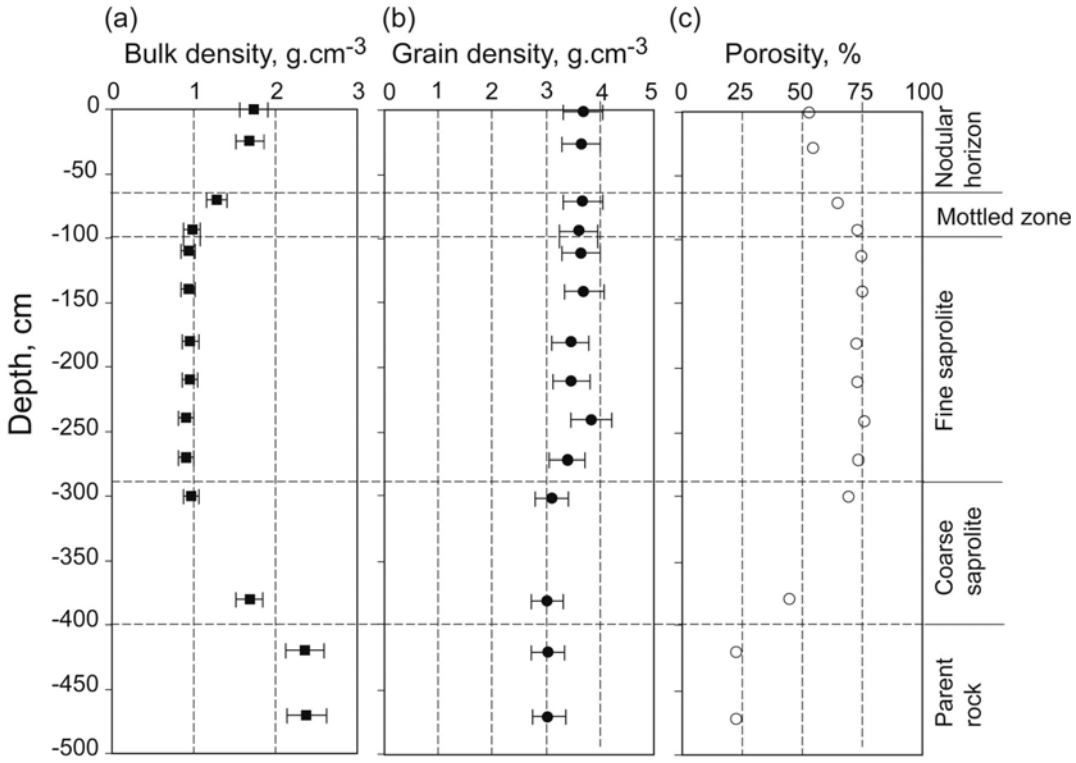

FIG. 3

524 *Traore et al., 2007*

525

525

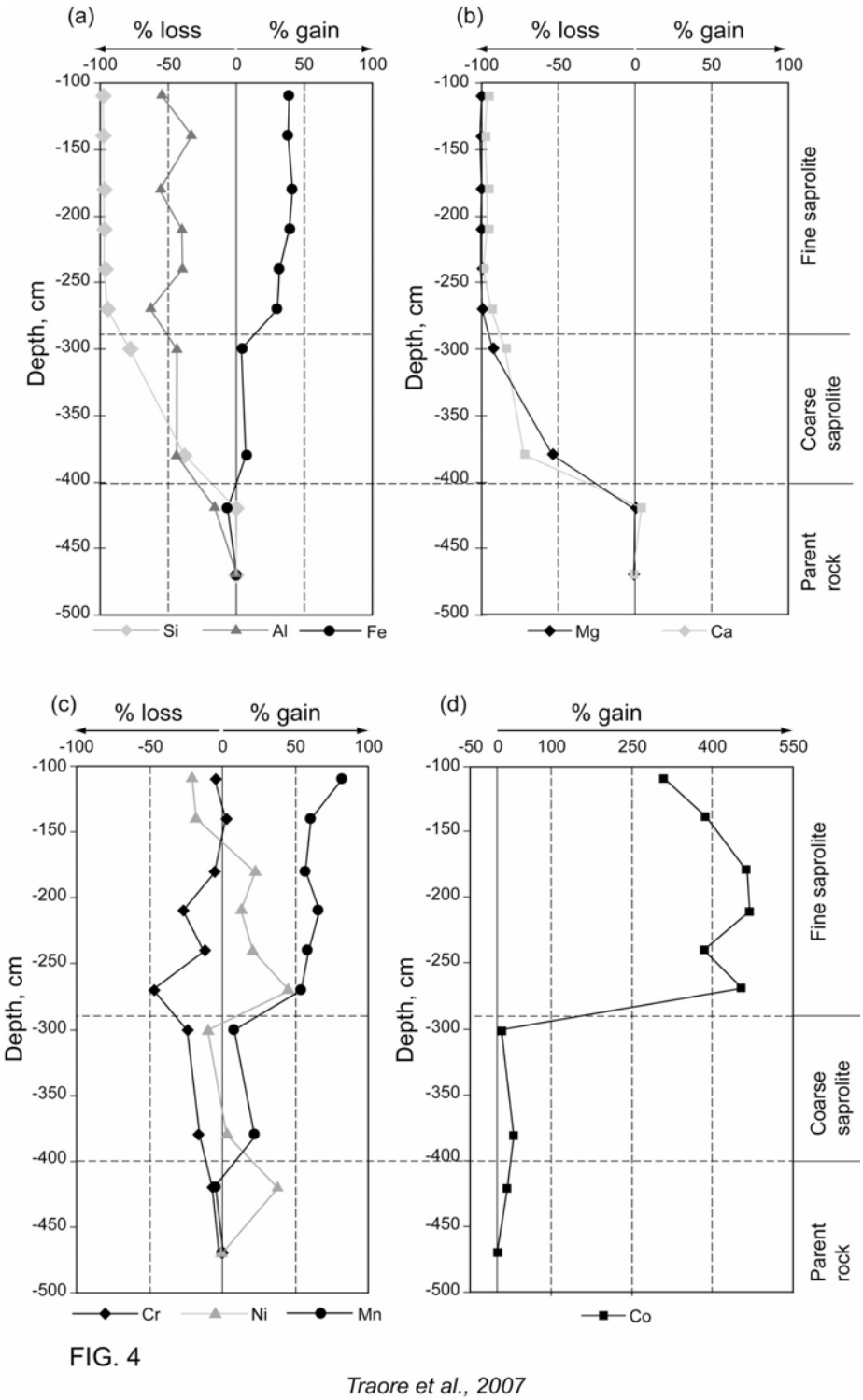

FIG. 4

526 *Traore et al., 2007*

527

527

528

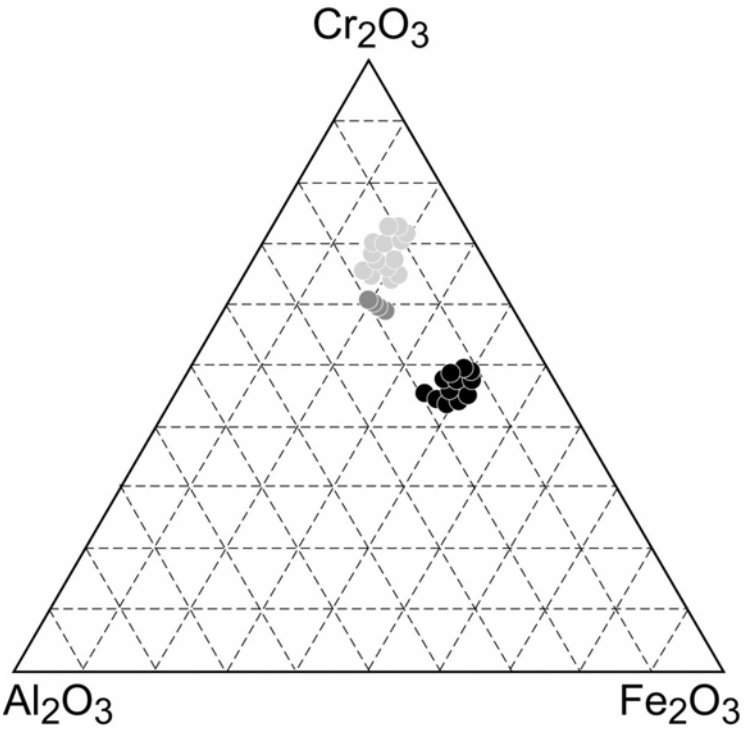

FIG. 5

529 *Traore et al., 2007*

530

531

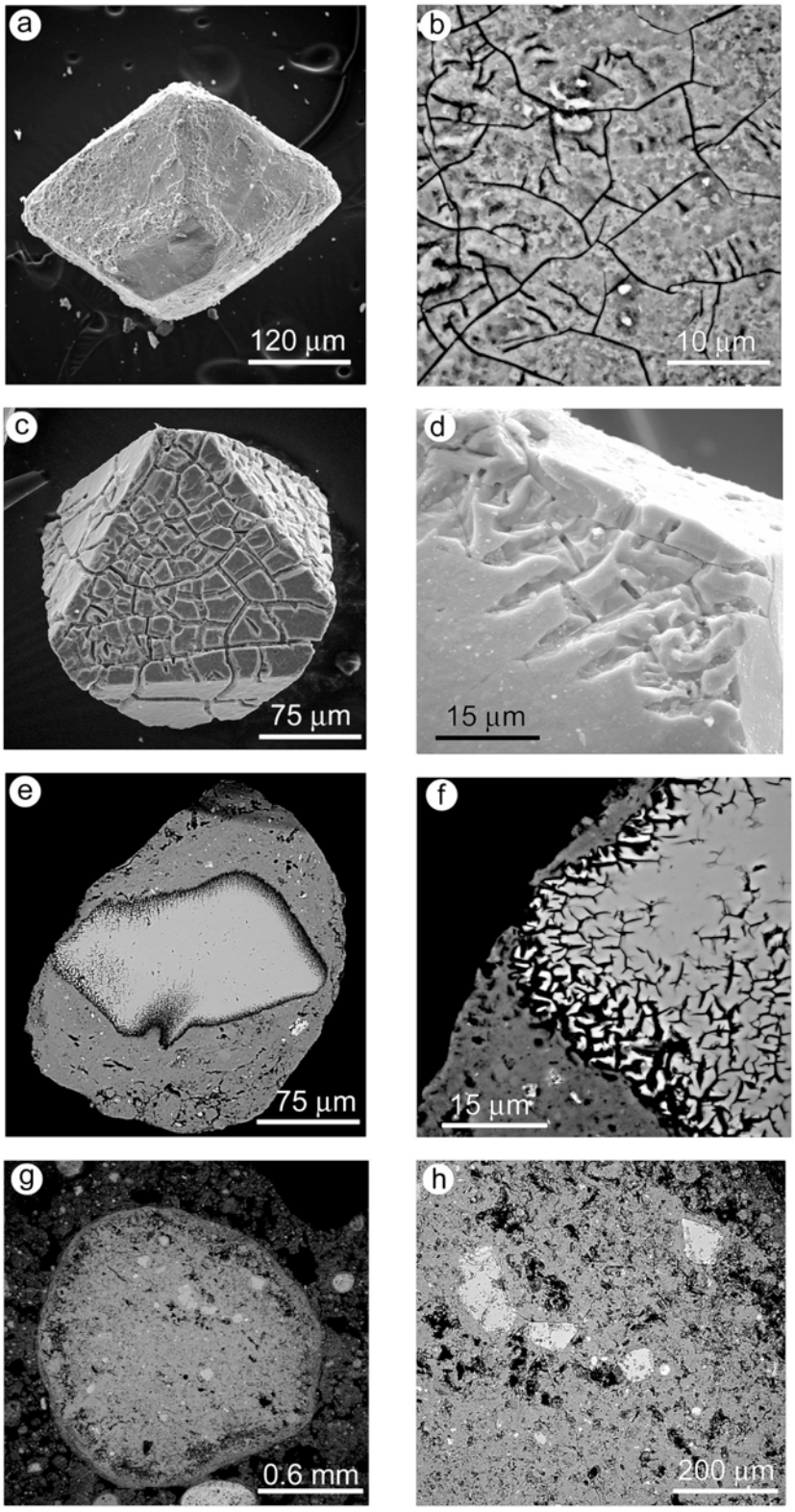

FIG. 6

Traore et al., 2007

531
532

532

533

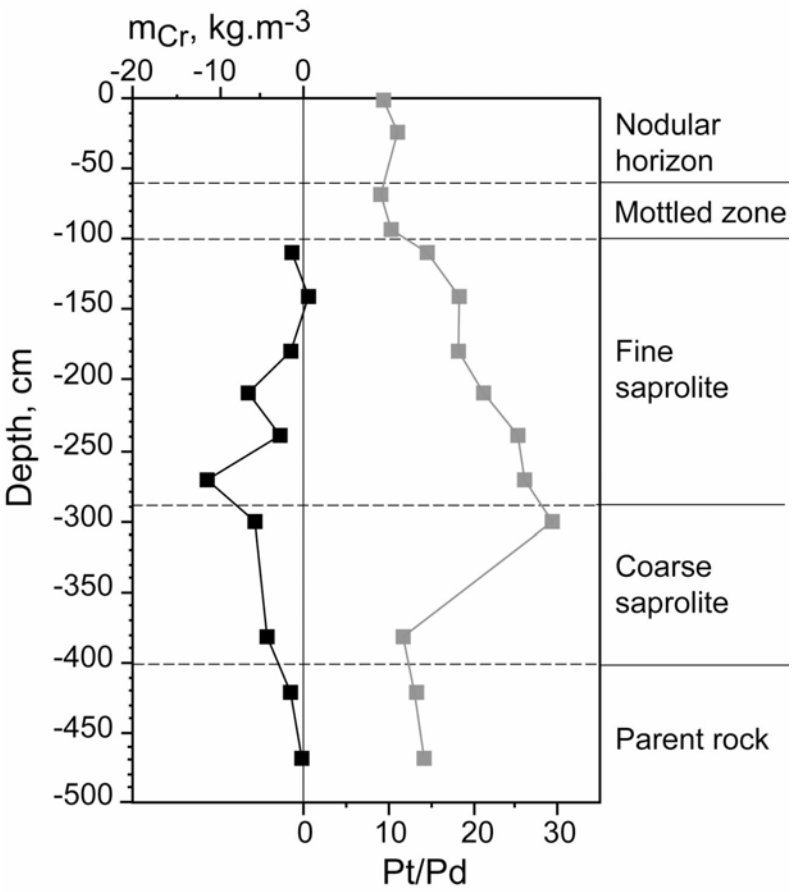

FIG. 7

534 *Traore et al., 2007*

	Uncertainty	Bedrock		Coarse saprolite		Fine saprolite						Mottled zone		Nodular horizon	
Sample n°		PG34	PG35	PG32	PG31	PG36	PG37	PG38	PG39	PG41	PG42	PG43	PG44	PW12	PW13
Depth (cm)		-470	-420	-380	-300	-270	-240	-210	-180	-140	-110	-95	-70	-25	0
ρ_w (g.cm^{-3})	± 0.1	2.38	2.36	1.68	0.97	0.91	0.91	0.95	0.96	0.93	0.93	0.98	1.28	1.69	1.73
ρ_g (g.cm^{-3})	± 0.1	3.06	3.04	3.02	3.11	3.39	3.84	3.47	3.45	3.70	3.65	3.60	3.68	3.65	3.69
Porosity (%)		22.22	22.37	44.37	68.81	73.16	76.30	72.62	72.17	74.86	74.52	72.78	65.22	53.70	53.12
SiO_2 (wt%)	± 0.01	39.48	39.81	34.65	21.27	6.00	4.08	3.32	2.99	2.20	2.07	2.09	1.88	2.10	1.90
Al_2O_3 (wt%)	± 0.01	0.68	0.58	0.56	0.97	0.67	1.09	1.02	0.75	1.17	0.80	2.43	0.95	4.30	4.20
Fe_2O_3 (wt%)	± 0.01	19.89	18.86	33.78	56.79	75.11	76.14	77.46	77.33	78.36	78.49	75.82	78.01	76.59	76.59
CaO (wt%)	± 0.01	0.34	0.36	0.14	0.14	0.07	0.02	0.05	0.05	0.03	0.05	0.02	0.03	0.01	0.02
MgO (wt%)	± 0.01	34.36	35.19	22.97	7.17	1.47	1.26	0.67	0.60	0.65	0.49	0.42	0.38	0.27	0.21
Cr_2O_3 (wt%)	± 0.01	1.54	1.45	1.82	2.88	2.14	3.56	2.84	3.62	4.06	3.76	4.85	4.42	2.05	2.01
LOI (wt%)	± 0.01	3.02	3.91	5.97	8.99	11.41	10.86	11.48	11.66	10.95	11.68	11.84	11.86	12.35	12.45
Total		99.31	100.16	99.89	98.21	96.87	97.01	96.84	97.00	97.42	97.34	97.47	97.53	97.67	97.38
Mn (mg/kg)	± 100	2012	1935	3483	5340	8127	8359	8359	7817	8282	9365	8514	9365	9690	9790
Co (mg/kg)	± 0.5	215	253	399	577	3140	2730	3080	3010	2670	2270	1950	1140	933	901
Ni (mg/kg)	± 5	2910	4040	4230	6430	11100	9190	8250	8820	6140	5960	6760	5530	5598	4802
Pd (µg/kg)	± 1	16	15	17	22	20	17	23	28	25	48	48	25	20	20
Pt (µg/kg)	± 0.5	227	206	204	647	527	440	483	497	442	683	497	241	225	196
Pt/Pd		14.18	13.75	12.00	29.43	26.37	25.90	21.00	17.74	17.68	14.23	10.35	9.68	11.25	9.80

TABLE 1

Traore et al., 2007

	Bedrock		Coarse saprolite		Fine saprolite					
Sample	PG34	PG35	PG32	PG31	PG36	PG37	PG38	PG39	PG41	PG42
Depth (cm)	-470	-420	-380	-300	-270	-240	-210	-180	-140	-110
(a)										
K_{Si} (%)	0.00	-0.01	-38.05	-78.04	-94.19	-96.05	-96.64	-96.95	-97.82	-97.95
K_{Al} (%)	0.00	-15.42	-41.87	-41.86	-62.33	-38.71	-40.13	-55.51	-32.77	-54.03
K_{Fe} (%)	0.00	-5.98	7.85	4.69	29.89	31.67	39.84	41.08	38.49	38.72
K_{Ca} (%)	0.00	4.99	-70.93	-83.22	-92.13	-97.75	-94.13	-94.07	-96.55	-94.25
K_{Mg} (%)	0.00	1.55	-52.81	-91.50	-98.36	-98.60	-99.22	-99.30	-99.26	-99.44
K_{Mn} (%)	0.00	-4.65	22.17	8.16	54.41	58.82	65.80	56.69	60.81	81.85
K_{Cr} (%)	0.00	-6.64	-16.58	-23.78	-46.87	-11.61	-26.39	-5.18	3.02	-4.59
K_{Ni} (%)	0.00	37.66	2.61	-9.94	45.85	20.75	13.16	22.26	-17.55	-19.97
K_{Co} (%)	0.00	16.69	31.00	9.38	458.41	385.50	471.82	464.71	385.26	312.57
(b)										
m_{Si} ($kg.m^{-3}$)	0.00	-0.05	-166.95	-342.45	-413.31	-421.47	-424.08	-425.40	-429.25	-429.81
m_{Al} ($kg.m^{-3}$)	0.00	-1.32	-3.58	-3.58	-5.34	-3.31	-3.44	-4.75	-2.81	-4.63
m_{Fe} ($kg.m^{-3}$)	0.00	-21.98	28.87	17.24	109.95	116.50	146.56	151.10	141.58	142.42
m_{Ca} ($kg.m^{-3}$)	0.00	0.29	-4.10	-4.81	-5.32	-5.65	-5.44	-5.43	-5.58	-5.45
m_{Mg} ($kg.m^{-3}$)	0.00	7.67	-260.42	-451.18	-485.05	-486.20	-489.28	-489.64	-489.47	-490.37
m_{Mn} ($kg.m^{-3}$)	0.00	-0.22	1.06	0.39	2.61	2.82	3.15	2.72	2.91	3.92
m_{Cr} ($kg.m^{-3}$)	0.00	-1.66	-4.16	-5.96	-11.75	-2.91	-6.62	-1.30	0.76	-1.15
m_{Ni} ($kg.m^{-3}$)	0.00	2.61	0.18	-0.69	3.18	1.44	0.91	1.54	-1.22	-1.38
m_{Co} ($kg.m^{-3}$)	0.00	0.09	0.16	0.05	2.35	1.97	2.41	2.38	1.97	1.60

TABLE 2